sustainability

MDPI

Article

Optimal Protection Scheme for Enhancing AC Microgrids Stability against Cascading Outages by Utilizing Events Scale Reduction Technique and Fuzzy Zero-Violation Clustering Algorithm

Hossein Karimkhan Zand [1], Kazem Mazlumi [1,*], Amir Bagheri [1] and Hamed Hashemi-Dezaki [2]

[1] Department of Electrical Engineering, Faculty of Engineering, University of Zanjan, Zanjan 45371-38791, Iran; karimkhan_zand@znu.ac.ir (H.K.Z.); a.bagheri@znu.ac.ir (A.B.)
[2] Department of Electrical and Computer Engineering, University of Kashan, Kashan 8731753153, Iran; hamed.hashemi@kashanu.ac.ir
* Correspondence: kmazlumi@znu.ac.ir

Abstract: The precision with which directional overcurrent relays (DOCRs) are set up establishes the microgrid customers' access to reliable and uninterrupted electricity. In order to avoid failure in DOCRs operation, it is critical to consider a single contingency (*N-1* event) on the protection optimization setting problem (POSP). However, power systems may face cascading outages or simultaneous contingencies (*N-K* events), which greatly expand the problem's complexity and scale. The effect of cascading events on this problem is an open research gap. Initially, this paper proposes a novel approach to reducing the scale of simultaneous events called the *N-K* events scale reduction technique (*N-K*-ESRT). Moreover, an innovative method named fuzzy zero-violation clustering is utilized to group these contingencies. Ultimately, the DOCRs' decision parameters are generated by three optimization algorithms, namely interior point (IPA), simulated annealing, and pattern search. In all case studies (including a real industrial network called TESKO2 feeder, the IEEE Std. 399-1997, and the IEEE 14 bus systems), the capabilities of the proposed method are effectively validated based on the DOCR's tripping time and the algorithm's execution time.

Keywords: microgrid; directional overcurrent relays (DOCRs); single contingency (*N-1* event); cascading outages (*N-K* events); protection optimization; event scale reduction technique; clustering algorithm

check for updates

Citation: Zand, H.K.; Mazlumi, K.; Bagheri, A.; Hashemi-Dezaki, H. Optimal Protection Scheme for Enhancing AC Microgrids Stability against Cascading Outages by Utilizing Events Scale Reduction Technique and Fuzzy Zero-Violation Clustering Algorithm. *Sustainability* **2023**, *15*, 15550. https://doi.org/10.3390/su152115550

Academic Editors: Luis Hernández-Callejo and Mohamed A. Mohamed

Received: 13 September 2023
Revised: 22 October 2023
Accepted: 30 October 2023
Published: 2 November 2023

Copyright: © 2023 by the authors. Licensee MDPI, Basel, Switzerland. This article is an open access article distributed under the terms and conditions of the Creative Commons Attribution (CC BY) license (https://creativecommons.org/licenses/by/4.0/).

1. Introduction

Generation, transmission, sub-transmission, and distribution networks are the four arms that constitute the whole electrical grid. The most critical and vital protective devices in distribution networks are overcurrent relays (OCRs) and DOCRs, which operate in the event of a fault. The fundamental task of protective relays is to quickly identify a permanent fault and transmit the tripping signal to the circuit breaker. The accurate setting of primary relays (main relays) is at the core of the fundamental architecture governing protective coordination, which is subsequently backed up by secondary relays (backup relays) at regular intervals. In traditional distribution networks, OCRs are the primary protection devices due to the radial orientation of the network's current [1,2]. The conventional electrical distribution network has recently been transformed into a microgrid as a consequence of the penetration of distributed generation (DG) units [3,4]. This resulted in the conception of microgrids, in which DGs can feed the distribution network with or without a power grid link [5,6]. Due to the multiple orientations of electric current in microgrids, protection schemes are based on DOCRs [7,8]. The DOCR setting parameters (*DSPs*) contain the current setting parameter (*CSP*) and the time setting multiplier parameter (*TSMP*).

The *TSMP* regulates the time required for the relay to trip, and the *CSP* is equal to the current flowing through the secondary side of the relay's current transformer (CT) [9,10]. The time-current characteristic of DOCRs is specified by both the current and time-setting parameters. Due to the nonlinearity of the POSP of DOCRs, nonlinear programming (NLP) is advised to answer the POSP [11,12]. In acknowledgment of the lack of advancement in heuristic and meta-heuristic optimization algorithms (MOAs) during the last decades, linear approaches (i.e., the simplex, two-phase simplex, and dual simplex programming) have been employed to assess the DOCR setting parameters [13]. In this literature, the POSP was formed using linear programming (LP) with the notion that one of the *DSPs* is given. In recent years, MOAs have been widely deployed to swiftly handle NLP without damaging the convexity of POSP. The noteworthy MOAs that have been employed to figure out the best outcomes of POSP include improved firefly optimization algorithm (IFOA) [9], improved moth-flame optimization algorithm (IMFOA) [10], imperialistic competition optimization algorithm (ICOA) [11], improved seagull optimization algorithm (ISOA) [12], chaotic search class topper optimization algorithm (CSCTOA) [13], the genetic algorithm (GA) [6,8,14–17], grey wolf optimization algorithm (GWOA) [17], and partial swam optimization (PSO) [15,18].

The disadvantages of MOAs, such as their penchant for early convergence at local points and the excess time needed to solve the POSP, can be alleviated by applying hybrid algorithms [19,20]. The outcomes achieved by hybrid algorithms in the referenced literature reveal the superiority of these techniques over others in tackling the malfunction of the DOCRs. In hybrid algorithms, the POSP is partitioned into sub-problems, each of which is addressed using a distinct strategy. In recent studies, hybrid algorithms, such as the hybrid whale optimization algorithm (HWOA) [19], GA-LP [20,21], PSO-LP [20], hybrid simulated annealing optimization algorithm (SAOA) and LP (HSAOA-LP) [22], hybrid ant colony optimization algorithm (HACOA) [23], hybrid gradient-based optimizer (HGBO) [24,25], hybrid opposition-based learning fractional order class topper optimization algorithm (HOBL-FOCTOA) [26], IPA [27], firefly algorithm (FA) and target remedy [28], fuzzy logic and GA [29], GA-PSO with differential evolution (DE) algorithm (GA-PSO-DE) [30], and FA-LP [31] have been devised. In addition, machine learning approaches facilitate the computation of *DSPs*. Furthermore, ref. [4] designed a protection scheme based on deep reinforcement learning (DRL) and long short-term memory (LSTM)-enhanced deep neural networks. Also, refs. [5–8] provided the clustering algorithms to group diverse network topologies into a small subset with k-means, pre-computed offline setup groups with storing memory, and self-organizing maps (SOM). To remedy the problem of low fault current contributions of inverter-based DGs (IBDGs), ref. [1] intends harmonic DOCR (HDOCR) with leveraging the current injection capability of IBDGs; ref. [2] exemplifies a third harmonic voltage produced by the IBDGs controller throughout fault currents; and ref. [3] refers to virtual impedance-fault current limiters (IFCLs).

The conventional methods of POSP were founded on the immutability of the grid topology (fixed topology (FT)). Nonetheless, electrical equipment failures (i.e., outages of lines, loads, DGs, synchronous machines, etc.) may alter the structure of the distribution grid [3]. This issue causes the *CSP* and fault currents of the network to fluctuate, ultimately resulting in incorrect relay operation [5,6]. To prevent the violation (i.e., miscoordination) of DOCRs, the literature advocated incorporating contingencies such as line outages [32], DG outages [33,34], a single contingency for all presumed equipment [3], and an islanding mode [1–3] into the POSP.

Hence, a comprehensive literature review is provided in Table 1 to establish the existing knowledge and gaps for microgrid protection in terms of published year, dual-setting DOCR, double inverse characteristic of DOCR, and multiple setting groups (MSGs).

Table 1. Summary of the literature review in the field of POSP of DOCR.

Reference	Year	Dual-Setting	Double Inverse	MSGs	HDOCR	SCD	N-SCD	SSSCD	FT	*N-1* Contingency	*N-2* Contingencies	Islanded Mode	PCAC	MOOP	Optimization Algorithm
[1]	2020	✗	✗	✗	✔	✗	✗	✗	✔	✗	✗	✔	✗	✗	-
[2]	2020	✗	✗	✗	✔	✗	✗	✗	✔	✗	✗	✔	✗	✗	-
[3]	2021	✗	✗	✗	✔	✗	✗	✗	✔	✔	✗	✔	✔	✗	-
[5]	2022	✗	✗	✔	✗	✔	✗	✗	✔	✔	✗	✔	✗	✗	-
[6]	2018	✗	✗	✔	✗	✔	✗	✗	✔	✔	✗	✗	✗	✗	GA
[7]	2021	✗	✗	✔	✗	✔	✗	✗	✔	✔	✗	✗	✗	✔	-
[9]	2019	✗	✗	✗	✗	✔	✗	✗	✔	✗	✗	✗	✗	✗	IFOA
[10]	2020	✗	✗	✗	✗	✔	✔	✔	✔	✗	✗	✗	✗	✗	IMFOA
[11]	2021	✗	✗	✗	✗	✔	✗	✗	✔	✗	✗	✗	✗	✗	ICOA
[12]	2022	✗	✗	✗	✗	✔	✗	✗	✔	✗	✗	✗	✗	✗	ISOA
[13]	2022	✗	✗	✗	✗	✔	✗	✗	✔	✗	✗	✗	✗	✗	CSCTOA
[14]	2018	✗	✗	✗	✗	✔	✗	✔	✔	✗	✗	✗	✗	✗	GA
[16]	2023	✔	✗	✗	✗	✔	✗	✔	✔	✗	✗	✔	✗	✗	GA
[17]	2022	✔	✗	✗	✗	✔	✗	✔	✔	✗	✗	✗	✗	✗	GA/GWOA
[18]	2023	✗	✗	✗	✗	✗	✔	✗	✔	✗	✗	✗	✗	✗	PSO
[19]	2019	✗	✗	✗	✗	✔	✗	✗	✔	✗	✗	✗	✗	✗	HWOA
[20]	2021	✗	✗	✗	✗	✔	✗	✗	✔	✔	✗	✔	✗	✗	GA-LP/PSO-LP
[21]	2019	✗	✗	✗	✗	✔	✗	✗	✔	✔	✗	✗	✗	✔	GA-LP
[22]	2020	✗	✗	✗	✗	✔	✗	✗	✔	✗	✗	✗	✗	✗	HSAOA-LP
[23]	2019	✗	✗	✗	✗	✔	✗	✗	✔	✗	✗	✗	✗	✗	HACOA
[24]	2021	✗	✗	✗	✗	✔	✗	✗	✔	✗	✗	✗	✗	✗	HGBO
[25]	2022	✗	✗	✗	✗	✔	✗	✔	✔	✗	✗	✗	✗	✗	HGBO
[26]	2021	✗	✗	✗	✗	✔	✗	✗	✔	✗	✗	✗	✗	✗	HOBL-FOCTOA
[27]	2019	✗	✗	✗	✗	✔	✗	✗	✔	✗	✗	✗	✗	✔	IPA
[28]	2021	✗	✗	✗	✗	✔	✔	✗	✔	✗	✗	✗	✗	✗	FA-Target Remedy
[29]	2023	✗	✗	✗	✗	✔	✔	✗	✔	✗	✗	✗	✗	✗	GA-Fuzzy Logic
[30]	2020	✗	✗	✗	✗	✔	✔	✔	✔	✗	✗	✗	✗	✗	GA-PSO-DE
[31]	2022	✗	✗	✗	✗	✔	✔	✗	✔	✗	✗	✗	✗	✗	FA-LP
[32]	2022	✗	✗	✗	✗	✔	✗	✗	✔	✔	✗	✔	✗	✗	HGA-LP

- stands for no data.

DOCR, HDOCR, standard characteristic of DOCR (SCD), non-standard characteristic of DOCR (N-SCD), smart selection of SCD (SSSCD), FT, *N-1* contingency, *N-2* contingencies, island mode, POSP of DOCR based on communication assisted scheme (PCAC), multi-objective optimization of problem (MOOP), and optimization algorithm.

In this table, the literature review has been summarized. As seen, there is a research gap in the literature because *N-2* contingencies have not been studied in the available references in the POSP of DOCR.

In previous decades, a blackout occurred in Europe on 4 November 2006, and in India on 30–31 July 2012, as a result of cascading events [35,36]. The following report excerpt is also included in [37], which contains the annual report for Nordic and Baltic system disruption statistics in 2020.

"Bus 1 (420 kV) in Halden was out of service due to a circuit breaker failure in Sweden. Simultaneously, Bus 2 (420 kV) in Halden is out of service for maintenance. Due to these events, 310 MWh of energy were not supplied, including the interruption of 240 MW of industrial load such as the production of paper".

Consequently, according to the cited literature and a recent report of power grid disturbances, simultaneous events result in a significant grid disconnection. The possibility of these occurrences is imminent and will result in substantial economic and reliability losses for sensitive loads.

In this paper, the DOCR setting parameters are determined by evaluating *N-2* contingencies in order to safeguard the network against a blackout. Cascading failures dramatically increase the problem model's complexity and size. In order to reduce the dimensions of the POSP, an innovative technique named *N-K*-ESRT is offered. As a result of this technique's foundation, all contingency scenarios are reduced to a much smaller subset, and the POSP only analyzes these chosen contingencies. Subsequently, an innovative clustering technique, namely the fuzzy zero-violation clustering algorithm (F-ZVCA), is applied to group the chosen contingencies in order to avoid the miscoordination of DOCRs. The IPA, SAOA, and pattern search optimization algorithm (PSOA) are ultimately employed to pinpoint the *DSPs* for each cluster. The most noteworthy contributions of this paper might be summarized as follows:

- An innovative scale reduction technique called *N-K*-ESRT is utilized to decrease the scale of the *N-2* contingencies.
- The F-ZVCA is proposed to eradicate the DOCR's miscoordination and reduce the scope of the POSP.
- The distinguish MOAs are recommended for determining the best *DSPs*.
- The offered solving procedure is applied to three AC microgrids, including a real distribution system (named TESKO2 feeder), besides the IEEE Std. 399-1997 and IEEE 14 bus systems.

2. Problem Modeling of DOCRs

The major purpose of the objective function (*OF*) is to decrease the operating time of the installed DOCRs while preventing miscoordination. Despite this, when cascading failures are factored into the POSP, the likelihood of DOCR's miscoordination skyrockets compared to a single outage. Consequently, during the optimization procedure, one of the major challenges is to completely eradicate the miscoordination of DOCRs. The *OF* of the problem model (1) and the associated relations and constraints, including the operation time of DOCRs (2), the miscoordination relation (3), the miscoordination constraint (4), the *TMSP* constraint (5), and the *CSP* constraints (6)–(7), are stated below. Also, it should be highlighted that all aforementioned relations (i.e., (2)–(7)) must be established for all network structures (i.e., index *S*), all main relays (i.e., index *M*), and their backup relays (i.e., index *JB*).

2.1. Objective Function

The objective function of the problem consists of two parts in (1). The prime focus of the first part is to optimize the operation time of all DOCRs. In fact, part 1 is the total operating time of all DOCRs that are installed in the related case study. On the other hand, the key aim of part 2 is to eliminate DOCR miscoordination between the primary DOCR and its backup relays. In actuality, invalid *DSPs* significantly increase the value of the *OF* (due to the penalty factor), and the problem model initially aims to eliminate this barrier by minimizing part 2. η is used as the penalty factor of the *OF* to prohibit miscoordination (or invalid *DSP*) that results in a negative δT. Following this, the problem model designates

the *DSPs* that are attempting to optimize the initial part among those that have contributed to the precise coordination of part 2. The *OF* can be represented by the following equation:

$$\left\{ OF = Optimization\left(\frac{\left\langle \sum_{M=1}^{Q} (T^{M,S}) \right\rangle}{part\ 1} + \frac{\langle \eta \times \delta T^{MJB,S} \rangle}{part\ 2}\right) \right\} \quad (1)$$

2.2. DOCRs Relations and Constraints

Equation (2) is the operating time (tripping time) of DOCR based on the inverse time characteristic of the *IEC 60255-3* standard [5]. The operating time of the relay is dependent on the *DSPs* and the fault current passing through the *Mth* relay (I_{FC}). The values of *DSPs* are directly proportional to the DOCR's operational time. In contrast, assuming the *DSPs* are fixed, (2) demonstrates that the operation time of DOCRs is inversely proportional to the fault current magnitude. Fault current is considered the near-end three-phase to ground faults.

As was previously established, the cornerstone of the POSP is the accurate setting of DOCRs without miscoordination and the minimization of the *OF*. Miscoordination occurs when a backup relay works before its primary relay. Due to the possibility of system lags such as a time delay in DOCR's CT, the miscoordination relation (3) considers 0.2 s as the time gap between the operation time of the primary relay and its backup DOCRs, which is called the coordination time interval (CTI). Moreover, η is employed as the penalty factor of the POSP to prohibit the miscoordination that leads to violation of the miscoordination constraint (i.e., negative δT), which is stated as (4).

In addition, (5) and (6) provide the upper and lower bounds for *CSP* and *TSMP*, respectively. The *TSMP* is modified in increments of 0.01 s between 0.05 s and 1 s. Furthermore, the *CSP* limit is between 0.1 A and 4 A, in increments of 0.1, assuming the current on the secondary side of the CT is 1 A. The boundary limits for *TSMP* and *CSP* are specified by the relay manufacturers. Here, the presumed DOCR is the SIPROTEC (i.e., Siemens protection relays) 7SJ64 multifunction numerical overcurrent relay, a Siemens manufacturing product [38]. Also, POSP in this paper is expressed as mixed integer nonlinear programming (MINLP) since *CSP* and *TSMP* are characterized discretely and continuously, respectively. Consequently, *TSMP* and *CSP* must be within the indicated range and adhere to the other limitations.

Another major limitation on the problem formulation is (7), in which the *CSP* through the *Mth* relay must be between the maximum load current ($I_{Loadmax}$) and the minimum fault current (I_{FCmin}). The far-end single-phase to ground fault is evaluated as the minimal fault current. Besides, the maximum load current equals the network current plus 20%. The DOCR relationships and constraints can be expressed as follows:

$$\left\{ T^{\mu,S} = \left\langle \frac{0.14 \times TSMP^{\mu,S}}{((\frac{I_{FC}^{\mu,S}}{CSP^{\mu,S}})^{0.02} - 1)} \right\rangle, \forall \mu, \forall S \right\} \quad (2)$$

$$\left\{ \delta T^{MJB,S} = \left\langle T^{JB,S} - T^{M,S} - 0.2^{\text{sec.}} \right\rangle, \forall (M, JB), \forall S \right\} \quad (3)$$

$$\left\{ \left\langle \delta T^{MJB,S} \geq 0 \right\rangle, \forall (M, JB) \in \mu, \forall S \right\} \quad (4)$$

$$\left\{ \left\langle 0.05, \leq, TSMP^{\mu,S}, \leq, 1 \right\rangle, \forall \mu, \forall S \right\} \quad (5)$$

$$\left\{ \left\langle CSP_{min}^{\mu,S} = 0.1 \leq CSP^{\mu,S} \leq 4 = CSP_{\max}^{\mu,S} \right\rangle, \forall \mu . \forall S \right\} \quad (6)$$

$$\left\{\left\langle I_{Loadmax}^{\mu,S} \le CSP^{\mu,S} \le I_{FCmin}^{\mu,S}\right\rangle, \forall\mu, \forall S\right\} \quad (7)$$

3. Protection Optimization Setting Problem

The POSP is divided into four parts, as shown in Figure 1. The *N-K*-ESRT as Part A (Section 3.1) is initially applied to *N-2* contingencies, and the chosen contingencies are identified. After that, the limitations of *CSP* are determined by the procedure described in Part B (Section 3.2). Next, F-ZVCA is performed to group the findings of *N-K*-ESRT in Part C (Section 3.3). In conclusion, MOAs will optimize the values of *DSPs* as Part D (Section 3.4). Each part is described in depth below.

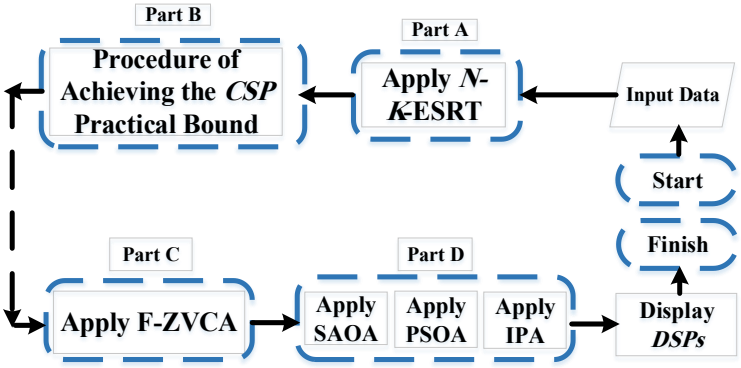


Figure 1. Flowchart of the POSP.

3.1. N-K Events Scale Reduction Technique

Professional standards mandate that microgrids be safeguarded against a single event, or *N-1* contingency [39–41]. Nevertheless, it is conceivable that *K* events occurred simultaneously, which is alluded to as *N-K* contingencies. Technically, the POSP does not need to take into consideration the three or four simultaneous outages ($K \geq 3$). This is due to the fact that the probabilities of these component failures are multiplied by each other, and the possibility of such occurrences is exceedingly low [42]. The incidence of *N-2* contingencies results in the disconnection of critical industrial loads and a sharp rise in energy not supplied (ENS) [43–45]. In light of this, the POSP of DOCRs is assessed, considering *N-2* events. However, managing *N-2* contingencies is significantly more difficult due to their vast number, especially in large-scale systems. Accordingly, the *N-K*-ESRT is recommended as an innovative solution to this problem. Due to the construction of *N-K*-ESRT, the number of all *N-2* probable events will greatly decrease. The *N-K*-ESRT puts all supposed outage-related equipment (lines, DGs, generators, etc.) into a subset. Next, the maximum and minimum voltage limits of each network's bus are calculated for all *N-2* outages. Following this, the process selects the *N-2* outages that result in the highest and lowest voltages for each bus. Given that the amount of current flowing through a line is directly proportional to the voltage difference between its corresponding buses, this technique encompasses the entire spectrum of network currents for all *N-2* events.

Consider Figure 2 as a sample network for judging this approach.

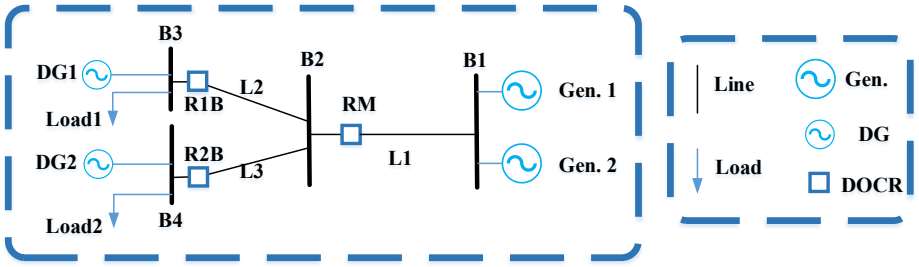


Figure 2. Sample network.

All anticipated equipment for *N-2* contingencies in a subset consists of nine components, including DG1 and DG2, load 1 and load 2, lines (i.e., L1, L2, and L3), and generators (i.e., Gen. 1 and Gen. 2). In order to implement the intended technique, the earlier specified equipment must be taken out of service in two simultaneous events, and the voltage of the buses (i.e., B1, B2, B3, and B4) must be measured in each of these occurrences. For example, one of the *N-2* events led to the lowest voltage value in B1, and another led to the highest voltage value in the same bus. The *N-K*-ESRT has picked these two occurrences as the chosen contingencies for B1. The POSP automatically applies this approach to each bus, resulting in eight occurrences based on (8) for the sample network's buses (i.e., NU^{ESRT} equals two times the number of buses in the network under investigation). Rather, if all *N-2* outages are considered, 36 occurrences (called *OCC*) will need to be investigated as (9) [46]. POSP is able to access the "maximum voltage violation study" for cascading events with the help of the Power Factory 15.1.7 DIgSILENT software. The result of this analysis reveals which of these 36 scenarios has the greatest and least noticeable impact on the network bus voltage. So, this method has led to a 75% decrease in the number of *N-2* events in the sample network, which would help reduce the size of the problem and speed up the POSP. It should be emphasized that, with the rise of assuming equipment for *N-2* events, this technique will be more beneficial than before.

$$\left\{ NU^{ESRT} = \left\langle \sum_{NB=1}^{NAB} 2 \times NB \right\rangle \right\} \tag{8}$$

$$\left\{ OCC = \left\langle \frac{N!}{(N-2)! \times 2} \right\rangle \right\} \tag{9}$$

3.2. The Procedure of Achieving the CSP Practical Bound (PA-CSP-PB) for the POSP

To facilitate the description of this section, Figure 2 serves as the sample network (as depicted in the *N-K*-ESRT section), and Figure 3 (consisting of parts A–K) provides the flowchart of PA-*CSP*-PB. The idea of this section is to acquire the *CSP* practical range of R_M (shown in Figure 2) according to (6) and (7), which can be applied to the rest of the DOCRs. First, the maximum network current passing through the R_M is used to determine the least bound of (7) for the R_M. This is accomplished by employing the Newton–Raphson load flow (NR-LF) to compute the current flowing through L1 (seen in part A).

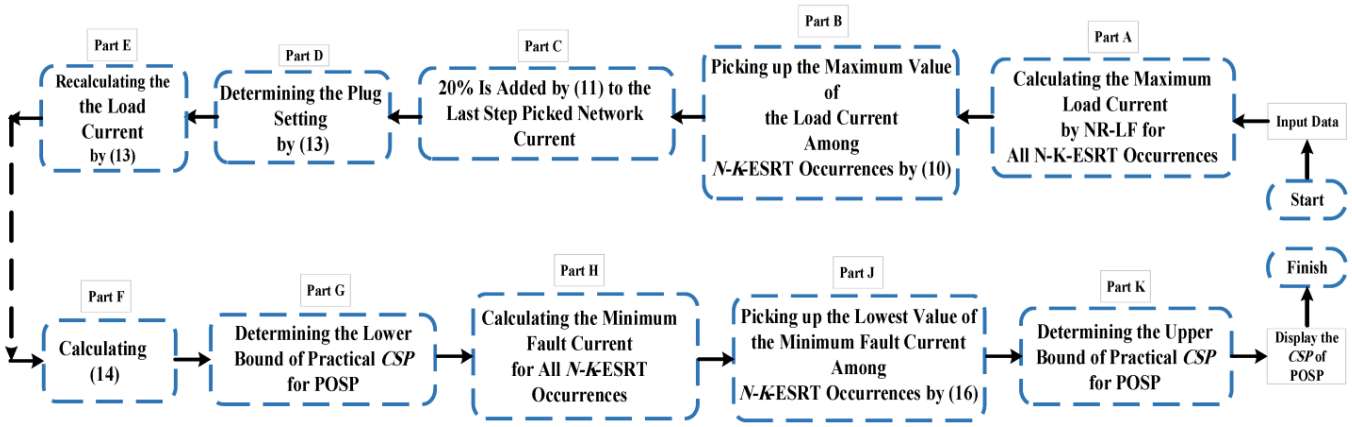


Figure 3. Flowchart of the PA-*CSP*-PB.

The picked current for the next part (part B) is the maximum current passing through the L1 ($I^{R_M}_{Loadmax}$) for all eight network configurations, which is attained by (10). As described in the preceding section, the *N-K*-ESRT identifies eight occurrences of two simultaneous outages. Subsequently, $I^{R_M}_{Loadmax}$ among these eight occurrences, one is chosen as the R_M's maximum current. Additionally, (11) adds 20% to the $I^{R_M}_{Loadmax}$, named $I^{R_M}_{Pickup}$. This issue is

due to the necessity of preventing a false trip caused by a maximum load current rather than a permanent fault (shown in part C). As seen in part D, (13) obtains the plug setting (PS^{R_M}) for the following approach, using (12) as an asset. The plug setting is the percent of R_M's CT winding, which varies from 50% to 200% in 25% increments. The ratio between the primary (*CTP*) and secondary (*CTS*) windings of a CT is denoted by (12) and written as *CTR*. In accordance with PA-*CSP*-PB, the plug setting is rounded up and $I_{Pickup}^{R_M}$ is recalculated by (13) as part E. Next, the current flowing through the secondary side of the CT ($I_{CSP}^{R_M}$) is calculated using the formula (14) and is illustrated in part F. This current ($I_{CSP}^{R_M}$) is the same current that should be deemed the lowest bound in (7). Particularly, the relation specified in (15) will suffice as the *CSP* bound of POSP. Accordingly, the lower limit of (15) is the greatest value between $I_{CSP}^{R_M}$ and $CSP_{\min}$(seen in part G). Selecting the maximum value at the lower limit of (15) is intended to prevent network power interruptions. The upper limit of (15) also represents the least value between CSP_{max} and $I_{FCmin}^{R_M}$. Note that the minimal short circuit current (i.e., $I_{FCmin}^{R_M}$) employed in the case studies is equivalent to the single-phase ground fault current stipulated by standard *IEC 60909-2001* [47] (part H). Similar to the preceding process that established the lower limit of the *CSP*, the short circuit current value used in the next part is the lowest short circuit current among all *N-K*-ESRT's topologies based on (16) and depicted in part J. The fault current determined by (16) is the maximum bound of (7). Now, the upper limit of (15) is the minimum value between the $I_{FCmin}^{R_M}$ and CSP_{max} (part K). Considering that the L1 should be rendered inoperable in the event of a short circuit, the minimum value was set at the upper limit of (15). The PA-*CSP*-PB will perform all the described steps for each relay. The PA-*CSP*-PB relations can be defined as:

$$\left\{ I_{Loadmax}^{M,S} = MAX\left\langle I_{Loadmax}^{M,1}, I_{Loadmax}^{M,2} \ldots, I_{Loadmax}^{M,S} \right\rangle \right\} \tag{10}$$

$$\left\{ I_{Pickup}^{M} = \left\langle I_{Loadmax}^{M,S} \times 1.2 \right\rangle \right\} \tag{11}$$

$$\left\{ CTR^{M} = \left\langle \frac{CTP^{M}}{CTS^{M}} \right\rangle \right\} \tag{12}$$

$$\left\{ PS^{M} = \left\langle \frac{I_{Pickup}^{M}}{CTP^{M}} \times 100 \right\rangle \right\} \tag{13}$$

$$\left\{ I_{CSP}^{M} = \left\langle \frac{I_{Pickup}^{M}}{CTR^{M}} \times 100 \right\rangle \right\} \tag{14}$$

$$\left\{ \left\langle MAX(CSP_{min}^{M,S}, I_{CSP}^{M}) \right\rangle \leq CSP^{M,S} \leq MIN(CSP_{max}^{M,S}, I_{FCmin}^{M,S} \right\rangle \} \tag{15}$$

$$\left\{ I_{FCmin}^{M,S} = MIN\left\langle I_{FCmin}^{M,1}, I_{FCmin}^{M,2} \ldots, I_{FCmin}^{M,S} \right\rangle \right\} \tag{16}$$

3.3. Fuzzy Zero-Violation Clustering Algorithm

Multiple setting groups are a function of the utilized relays that permit the DOCRs to have several *DSP* groups, only one of which operates in the present grid structure [5–8]. To employ DOCR's MSG, similar *DSPs* are placed in the right cluster using clustering algorithms. Given that there are four MSGs in DOCR, the *N-K*-ESRT must be divided into four clusters (or less than four clusters). Clustering is a mathematical technique for categorizing several similar data points into distinct groups [6]. As an innovative clustering algorithm, the F-ZVCA groups all topologies obtained by *N-K*-ESRT into separate clusters using the procedure outlined below. The concept of F-ZVCA comes from k-means clustering, fuzzy C-means clustering, and POSP trial and error.

Assigning each topology to its appropriate cluster involves the following six steps, which are shown in Figure 4:

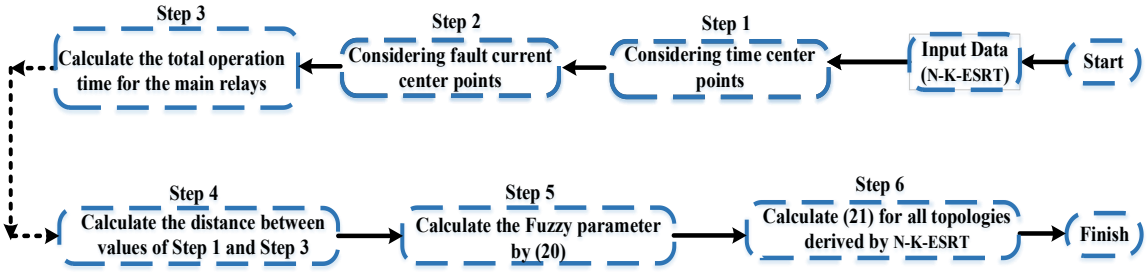


Figure 4. The diagram of F-ZVCA.

Step 1: Initially, time center points are randomly considered as the centers of the clusters (OT^{C1}, OT^{C2}, OT^{C3}, and OT^{C4}). These center points indicate the total operating time (OT) of the network's primary relays. For instance, OT^{C1} is identified as the time center point for the "*C1*" cluster (i.e., cluster 1).

Step 2: Secondly, fault current center locations designated λ^{C}(including λ^{C1}, λ^{C2}, λ^{C3}, and λ^{C4}) are picked at random as supplementary cluster centers. These center points reflect the total fault current ratio between the main DOCRs and their backup relays. In this particular case, the fault current centroid point of "*C2*" (i.e., cluster 2) is shown as λ^{C2}.

Step 3: Subsequently, the total operation time of the main relays is decided based on (17) for all derived topologies (OT^{S1}, OT^{S2}... etc.) with the help of (1) and the default $TSMP = 1$, and $CSP = I_{CSP}$. For example, OT^{S3} signifies the total operation time of the main DOCRs for the "*S3*" topology.

Step 4: Fourth, using (18), the distance of OT^{S1} from all time center points (i.e., OT^{C1}, OT^{C2}... etc.) is determined and designated as $DOT^{S1\text{-}C1}$, $DOT^{S1\text{-}C2}$, ... This procedure is done for each resultant topology (i.e., $DOT^{S2\text{-}C1}$... $DOT^{S3\text{-}C1}$...).

Step 5: Using the formula in (19), a fuzzy parameter denoted $\omega\lambda^{S-C}$ is derived by (20). Equation (19) signifies the average ratio between the fault current of the primary DOCR and their backup relays. λ^{S} is computed for any topologies coming from *N-K*-ESRT. In essence, (19) demonstrates that the fluctuations in the short-circuit level were significant for each topology; presumably, that topology should have a higher probability of being conveyed.

(Note: The resultant topologies should be more likely to be clustered together when the $\omega\lambda^{S-C}$ values are closest to each other among all ones.)

Step 6: Equation (21) is determined between each derived topology and the clusters using (20) and (18). Among the values obtained for topology '*S1*', including: $D\omega^{S1\text{-}C1}$, $D\omega^{S1\text{-}C2}$, ..., topology '*S1*' is allocated to the cluster with the smallest $D\omega^{S\text{-}C}$ value. Lastly, steps 1 through 6 are repeated until the clusters' constituents are no longer altered.

The F-ZVCA will therefore exhibit its results if the POSP has no miscoordination across all clusters. If miscoordination has occurred, F-ZVCA relocates the specific topology to a different cluster. As stated previously, the specified topology must be transmitted from its cluster to another cluster with the maximum possible value of (21). This topology should be transmitted to the succeeding cluster if (19) has the greatest value deviation compared to the other topologies generated by *N-K*-ESRT. The relationships associated with F-ZVCA can be described as follows:

$$\left\{ OT^{S} = \sum_{M=1}^{Q} \left\langle \frac{0.14 \times 1}{((\frac{I_{FC}^{M,S}}{I_{CSP}^{M,S}})^{0.02} - 1)} \right\rangle \right\} \tag{17}$$

$$\left\{ DOT^{S-C} = \left\langle \left| OT^{S} - OT^{C} \right| \right\rangle \right\} \tag{18}$$

$$\left\{\lambda^{S} = Avg\left\langle \sum_{M,JB} \frac{I_{FC}^{M,S}}{I_{FC}^{JB,S}} \right\rangle, \forall(M, JB), \forall S\right\} \tag{19}$$

$$\left\{\omega\lambda^{S-C} = \left\langle \frac{\left|\lambda^{S} - \lambda^{C}\right|}{\lambda^{C}} \right\rangle\right\} \tag{20}$$

$$\left\{D\omega^{S-C} = \left\langle \omega\lambda^{S-C} \times DOT^{S-C} \right\rangle\right\} \tag{21}$$

3.4. Meta-Heuristic Optimization Algorithms

After the *N-K*-ESRT and F-ZVCA reduce the dimensions of the POSP, the *DPSs* are produced employing three MOAs, encompassing IPA, SAOA, and PSOA. The IPA handles both vastness and spread as well as smallness and concentration problems and may be retrieved from either *NaN* or *Inf* results [48]. Besides, SAOA is a technique for answering both constrained and unconstrained optimization issues. Accepting poorer solutions throughout the optimization procedure while retaining the ability to escape local points is a distinguishing feature of SAOA [22]. On the other hand, PSOA is highly valuable for nonlinear programming problems and has the potential to substantially optimize local search. Refer to [22,48,49] for details on the IPA, SAOA, and PSOA, respectively.

4. POSP Setup

4.1. The Assumption about the POSP

Owing to the fact that the FT of the network is a stable state of the power grid and the power network is continually fluctuating between the FT and event-derived topologies, the FT has been deemed the default in all clusters. After trial and error in the problem-solving procedure, it has been proven that the I_{CSP} is always higher than the CSP_{min} and lower than the I_{FCmin} in all evaluated cases. Nevertheless, as examined and validated by Noghabi et al. [34], including both decision variables of DOCRs in the cycle of optimization algorithms merely slows down the convergence process of the problem. Therefore, the *CSP* is equivalent to the I_{CSP}, which will be produced by using PA-*CSP*-PB. As a result, the *CSPs* are the same across all clusters and are not cluster-dependent. The end criteria for POSP are *OF*'s tolerance and MOA's execution time (MET). The *OF*'s tolerance is presumed to be 1×10^{-16}, and the maximum limit of MET is set to 100 s, resulting in more accurate findings [50]. This section additionally provides the average tripping time (ATT), the ATT for one relay (ATTO), the maximum tripping time (MTT), the overall *TSMP* (O-*TSMP*), and the iteration of MOAs (IMA) to aid comprehension of the POSP. Furthermore, logarithmic indices have been utilized on numerous vertical and horizontal axes of the figure obtained from POSP in order to enhance the distance portrayal and coherence of the paper's figures.

4.2. N-K-ESRT and F-ZVCA Results: IEEE Std. 399-1997 System

As observed in Figure 5, the IEEE Std. 399-1997 network is made up of 19 buses (B1, . . ., B19), 20 lines (L1, . . ., L20), 14 loads (Load1, . . ., Load14), 26 relays (R1, . . ., R26), and 1 external grid (EX). This industrial network is connected to the EX through two 69 KV/13.8 KV transformers (T1 and T2) [51]. In particular, this system is linked to two DG units with capacities of 15.6 MVA and 12.5 MVA for DG1 and DG2, respectively. This network is scheduled to contain 39 pieces of equipment for *N-2* events (including all DGs, loads, lines, transformers, and Ex). There are 741 cases of *N-2* events, according to (9). However, in accordance with Table 2, only eleven occurrences are investigated by *N-K*-ESRT, which reduces the size of the POSP by 98.651%. Due to the availability of 16 buses on the distribution part of the Example St. 399-1997 network, the *N-K*-ESRT ought to provide 32 cases based on (8). Due to the frequent bus-related events (illustrated in Table 2 in the EN row), the *N-K*-ESRT results are limited to 11 modes as opposed to 32 modes. Table 2 indicates that the voltage of fixed topology (VFT) for bus 5 is 0.99 PU. The VFT increases to

the event voltage (EV) of 1 PU following the outages of L13-L9 (i.e., simultaneous outages for lines 13 and 9). In contrast, the VFT decreases to 0.94 PU as a result of the outages of lines 11 and DG1 (event name: EN). Notably, the aforementioned contingencies (L13 and L9 outages, L11 and DG1 outages) result in the lower (LB) and upper (UB) bounds of voltage ranges for bus 5 among all *N-2* occurrences. After defining the chosen contingencies by *N-K*-ESRT, the F-ZVCA is utilized in order to group these contingencies. As a result of F-ZVCA, Figure 6 depicts the clustering of the *N-2* contingencies into three clusters (Clusters 1–3). The maximum number of occurrences is allocated to cluster 1, which has nine topologies, indicating that these topologies are closer in terms of the short-circuit current based on (19). In addition, cluster 2 and cluster 3 only account for a single *N-2* contingency, which includes L11-DG1 and L6-DG2 outages, respectively.

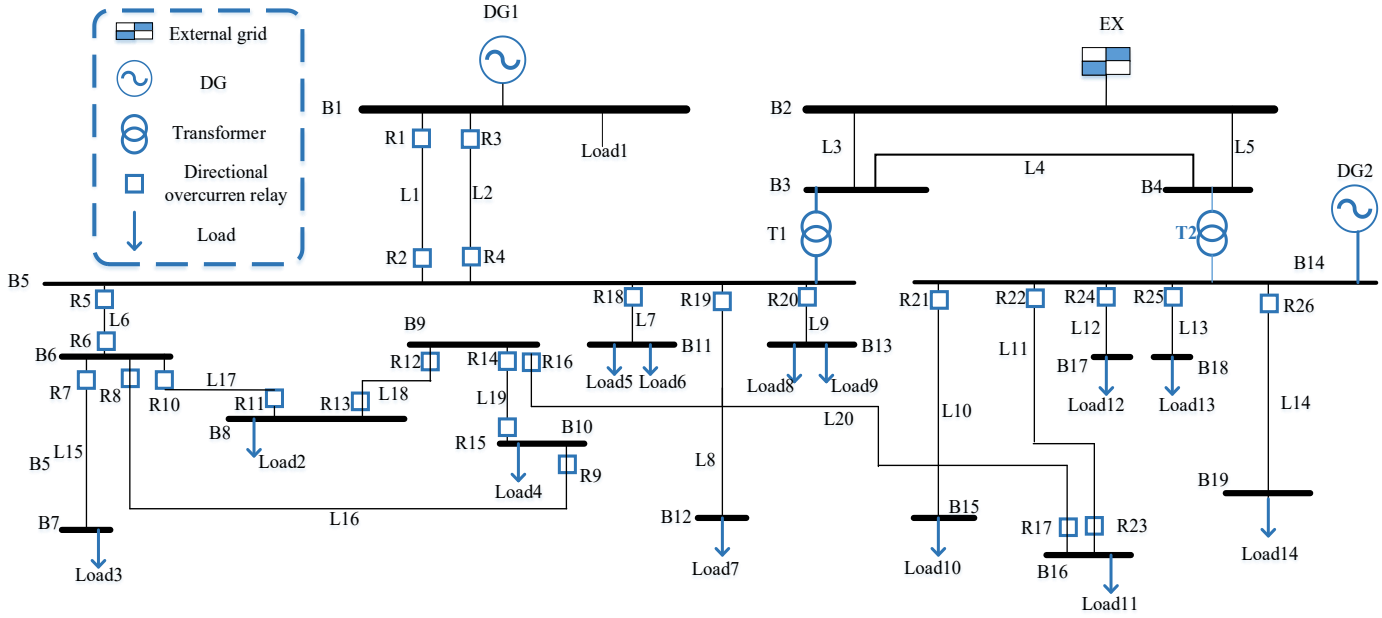


Figure 5. IEEE Std. 399-1997 system.

Table 2. Results of *N-K*-ESRT for the IEEE Std. 399-1997 system.

Bus	B1		B5		B6		B7		B8		B9		B10		B 11	
	LB	UB	LB	UB	LB	UB	LB	UB	LB	UB	LB	UB	LB	UB	LB	UB
EV	0.95	1	0.94	1	0.94	0.99	0.94	1	0.94	0.99	0.94	1	0.94	0.99	0.94	1
VFT	1		0.99		0.99		0.99		0.99		0.99		0.99		0.99	
EN	L11-DG1	FT	L11-DG1	L13-L9	L11-DG1	FT	L11-DG1	FT	L11-DG1	FT	L11-DG1	FT	L11-DG1	FT	L11-DG1	L9-Load5
Bus	B 12		B13		B14		B15		B 16		B17		B18		B19	
	LB	UB	LB	UB	LB	UB	LB	UB	LB	UB	LB	UB	LB	UB	LB	UB
EV	0.94	0.99	0.94	1	0.94	0.99	0.94	1	0.94	0.99	0.95	1	0.95	1	0.95	1
VFT	0.99		0.99		1		0.99		0.99		0.99		0.99		0.99	
EN	L11-DG1	FT	L11-DG1	L7-Load9	L11-DG1	FT	L11-DG1	L1-Load10	L11-DG1	L20-Load11	L6-DG2	L1-Load12	L6-DG2	L1-Load13	L6-DG2	L1-Load14

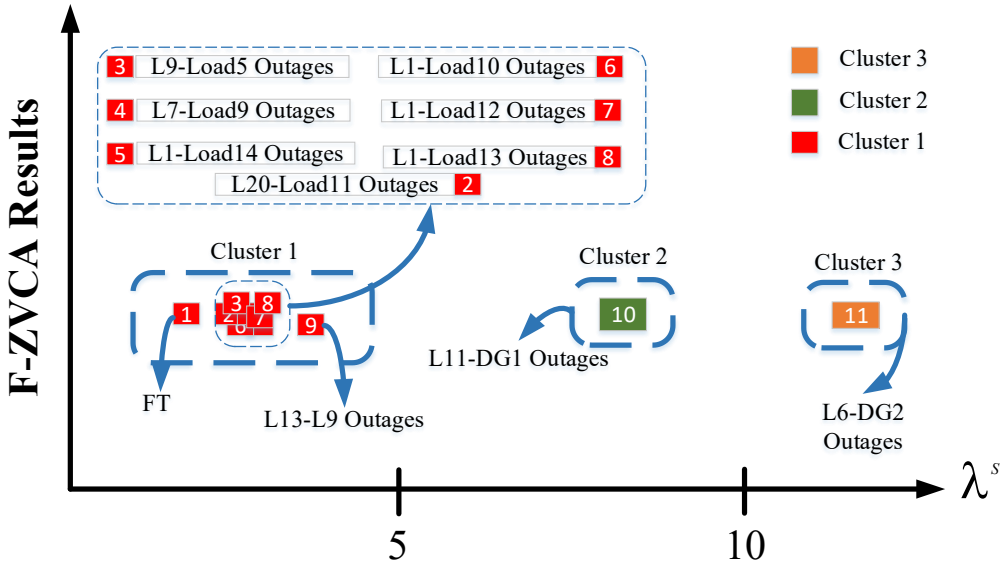


Figure 6. Results of F-ZVCA for the IEEE Std. 399-1997 system.

4.3. Simulation Results: IEEE Std. 399-1997 System

The SAOA and PSOA are not converged for the IEEE Std. 399-1997 system. The impediment clusters in the trend of convergence of SAOA and PSOA are clusters 3 and 1, respectively, which cause the POSP to be implemented in a way that is not coordinated. Given that the POSP is worthless if even a single DOCR of the clusters causes failure (i.e., one miscoordination is sufficient to render the POSP ineffective). In greater detail, in the case of miscoordination, the penalty variable (i.e., η) causes the *OF* to grow overly large, resulting in the POSP failing to converge. Despite the aforementioned algorithms, IPA's results among all three clusters are error-free, ending in a flawless convergence of POSP. As depicted in Figure 7, Tables 3 and 4, the optimized *OFs* of IPA for clusters 1, 2, and 3 are 314, 240, and 184.5, with 20, 85, and 19 IMA, respectively. Table 3 lists the *DSPs* accessed by IPA for all three clusters of the IEEE Std. 399-1997 system. It is crucial to highlight that optimal *DSPs* will enable the propensity of *OFs* to converge. This indicates that changes in *DSPs* have a direct impact on *OF* values. As seen in Table 3 and mentioned before, *CSPs* are the same throughout all clusters and are not cluster-dependent. Since each cluster has a specific set of limitations associated with its system topologies, the *TSMPs* are not identical between all clusters in the same way that *CSPs* are. According to Table 4, the O-*TSMP* (MTT, ATT, and ATTO) best achieved by IPA for clusters 1, 2, and 3 is 14.015 s (28.332 s, 28.229 s, and 1.085 s), 11.281 s (25.892 s, 25.892 s, and 1.078 s), and 10.147 s (21.22 s, 21.22 s, and 0.884 s), respectively.

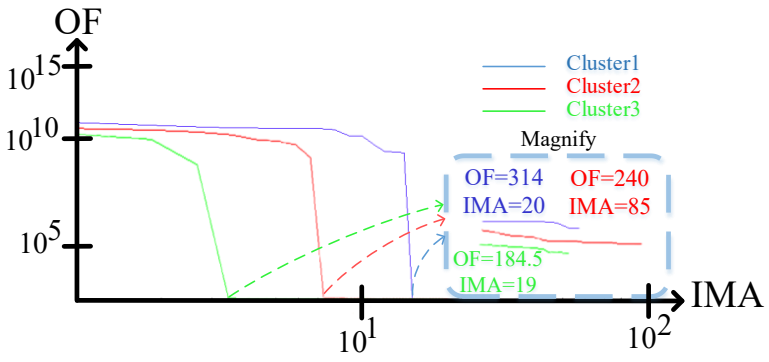


Figure 7. Convergence trend of the IPA in the IEEE Std. 399-1997 system.

Table 3. *DSPs* for the IEEE Std. 399-1997 system reached by IPA.

Relay		R1	R2	R3	R4	R5	R6	R7	R8	R9	R10	R11	R12	R13
CSP		1.8	1.8	1.8	1.8	1.4	1.4	1.4	1.4	1.4	2	2	1.6	1.6
TSMP	**Cluster 1**	0.39	0.427	0.399	0.427	0.691	0.381	0.49	0.847	0.49	0.876	0.509	0.595	0.529
	Cluster 2	0.392	0.454	0.391	0.456	1	0.583	0.84	0.964	0.05	0.994	0.052	0.113	0.667
	Cluster 3	0.471	0.05	0.471	0.05	0.557	0.999	0.356	0.45	0.05	0.667	0.05	0.285	0.508
Relay		**R14**	**R15**	**R16**	**R17**	**R18**	**R19**	**R20**	**R21**	**R22**	**R23**	**R24**	**R25**	**R26**
CSP		1.6	1.6	1.6	1.6	1.4	1	1	1.8	1.4	1.4	0.8	1.8	1.6
TSMP	**Cluster 1**	0.645	0.973	0.429	0.516	0.178	0.491	0.492	0.462	0.978	0.354	0.475	0.475	0.475
	Cluster 2	0.142	0.91	0.053	0.488	0.08	0.285	0.267	0.276	0.488	0.488	0.292	0.266	0.278
	Cluster 3	0.388	0.829	0.393	0.482	0.051	0.649	0.05	0.392	0.482	0.337	0.393	0.361	0.366

Table 4. Results of the IEEE Std. 399-1997 system reached by IPA.

System	O-*TSMP*	MTT	ATT	ATTO	*OF*	MET	IMA	TOFE
Cluster 1	14.015	28.332	28.229	1.085	314	1.8	20	715
Cluster 2	11.281	25.892	25.892	1.078	240	8.1	85	3010
Cluster 3	10.147	21.22	21.22	0.884	184.5	1.8	19	687

It is clear that cluster 1 has higher values for *OF*, O-*TSMP*, MTT, ATT, and ATTO than clusters 2 and 3. In light of this, the POSP is handled by the greatest number of topologies allocated to cluster 1 (seen in Figure 6), resulting in a more complex problem for cluster 1 than the other clusters. For extra information, POSP must be performed for each of the nine topologies assigned to cluster 1, and the aforesaid limitation must be met for all of them. In terms of short circuit level, the POSP of clusters 2 and 3 is much more relaxed than that of cluster 1. This advantage is exacerbated by the fact that clusters 2 and 3 cover just one of the *N-2* outages, yielding the smallest influence on fluctuations in short-circuit current. Therefore, cluster 1 has the longest tripping time relative to the other clusters due to the fact that the fault current is inversely proportional to the DOCR's tripping time based on (2). In addition, IPA's METs for clusters 1, 2, and 3 are 1.8 s, 8.1 s, and 1.8 s, respectively. These MET are extremely fast computation times that are appropriate for solving the POSP. Moreover, the total objective function evaluation (TOFE) determined by IPA for clusters 1, 2, and 3 is 715, 3010, and 687, as displayed in Figure 8 and Table 4. The TOFE refers to the number of *OF* evaluations throughout each iteration. For deeper inquiry, and as seen in Figure 8, cluster 1 has 31 TOFE in the first iteration and 50 TOFE in the last iteration. It should be noted that the MET of cluster 2 is 4.5 times longer than those of clusters 1 and 3, culminating in the TOFE of cluster 2, which is much bigger than those of clusters 1 and 3.

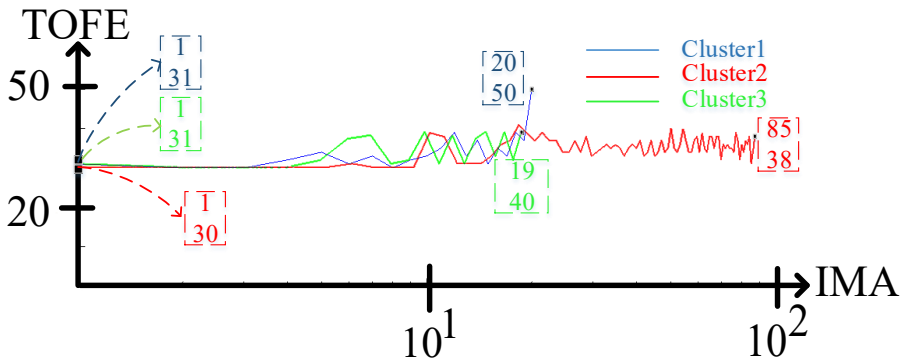


Figure 8. TOFE of the IPA in the IEEE Std. 399-1997 System.

4.4. Simulation Results: TESKO2 System

An industrial radial feeder designated as the TESKO2 feeder is represented in Figure 9. Actually, one of the sub-transmission substation's (which is considered an EX) outgoing feeders is the TESKO2 feeder, which is situated in northwest Iran.



Figure 9. Industrial TESKO2 System.

This system has three DGs (DG_a, DG_b, and DG_c) with a capacity of 2.2 MVA, five lines (L1, . . ., L5), three loads ($Load_a$, $Load_b$, and $Load_c$), and ten DOCRs (R_a, . . ., R_X). In the TESKO2 network, the presumed equipment for *N-2* events consists of 12 components, including all loads, synchronous machines, and lines, of which only five topologies are analyzed as *N-K*-ESRT. The repercussions of *N-K*-ESRT have involved $Load_a$-$Load_b$ outages, L1-L2 outages, DG_a-DG_c outages, DG_a-DG_b outages, and FT. If the F-ZVCA is employed, it is expected that all NU^{ESRT} occurrences are kept within a single cluster with zero miscoordination.

Therefore, the paucity of these topological quantities is the reason for the absence of clustering in this network. Despite the former case study, the TESKO2 system has converged across all MOAs (SAOA, PSOA, and IPA). As demonstrated in Figure 10 and Table 5, the converged *OF* of SAOA, PSOA, and IPA is 555.94 (with 1777 IMA), 262.97 (with 263 IMA), and 1300.85 (with 11 IMA), respectively. Additionally, Table 5 reveals the findings for MOAs' *DSPs*. In comparison to the earlier case study, it is anticipated that the ATT, ATTO, MTT, and O-*TSMP* will be attained with lower values for the TESKO2 system. The TESKO2 grid is a radial network, and as a result, the POSP limitations are far less severe than they are for the IEEE Std. 399-1997 system. As indicated in Table 5, the ATT attained by SAOA, PSOA, and IPA is 6.915 s, 4.562 s, and 9.432 s, respectively. As a result, the PSOA is the optimal solution in terms of average operation time for one DOCR, with a value of 0.456 s as ATTO. The O-*TSMP* values acquired by PSOA and IPA are 2.522 s and 5.236 s, respectively, which are the lowest and highest values ever observed. The IPA method is implemented disappointingly in terms of MTT and ATT, with values of 12.284 s and 9.432 s, respectively. Nevertheless, the algorithm with the lowest MET is the IPA, whose MET is faster than other MOAs. The MET achieved by IPA, PSOA, and SAOA is 1.1 s, 25.5 s, and 100 s, respectively. It should be emphasized that the upper bound of MET and the function tolerance are the end criteria for SAOA and IPA, respectively.

Table 5. Results of the TESKO2 system reached by MOAs.

Relay		R_a	R_b	R_c	R_d	R_e	R_f	R_g	R_h	R_i	R_x	All Relays						
CSP		1.8	1.8	1.8	1.8	1.4	1.4	1.4	1.4	1.4	2	O-*TSMP*	ATT	MTT	ATTO	*OF*	MET	IMA
TSMP	IPA	0.465	0.407	0.418	0.572	0.41	0.409	0.413	0.571	0.998	0.573	5.236	9.432	12.284	0.943	1300.8	1.1	11
	SAOA	0.128	0.067	0.389	0.486	0.216	0.067	0.266	0.259	0.547	0.366	2.796	6.915	11.198	0.691	555.9	100	1777
	PSOA	0.05	0.146	0.185	1	0.15	0.05	0.214	0.17	0.311	0.246	2.522	4.562	5.863	0.456	262.9	25.5	263

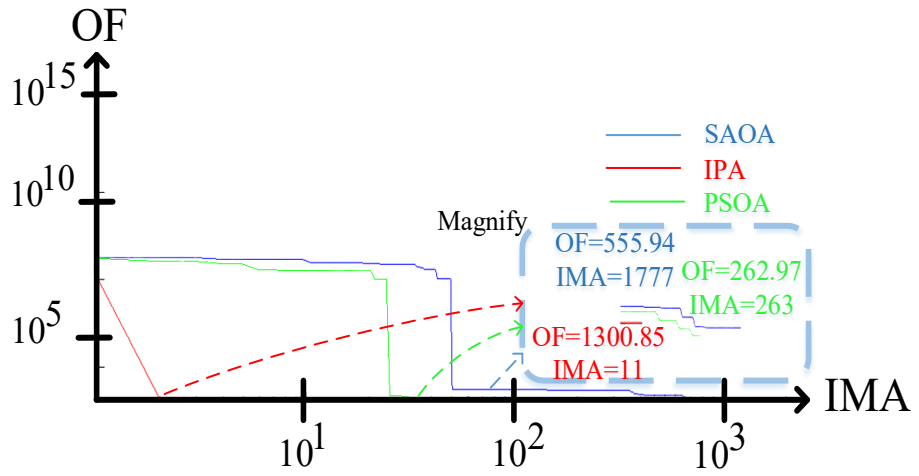


Figure 10. Convergence trend of the MOAs in the TESKO2 system.

Consequently, it can be stated that the IPA and PSOA have been deemed the privileged MOAs for the TESKO2 feeder in terms of MET and ATTO, respectively (Figure 11 represents the TOFE of these algorithms). As shown in Figure 11, the TOFE values for IPA and PSOA are 378 and 3527, respectively. Given that PSOA's MET is 23.18 times longer than IPA's (mentioned in Table 5), the TOFE of PSOA is dramatically higher than that of IPA. Moreover, it can be pointed out that the TOFE of IPA acquired for the IEEE Std. 399-1997 system has a growing trend compared to the TESKO2 feeder, which is due to the fact that the IEEE Std. 399-1997 network is notably more looped than the TESKO2 grid. In looped systems, it is considerably more challenging to satisfy *TSMP* and coordination constraints than in radial networks. Because of this concern, IMA and MET rise significantly, forcing meshed networks to have a higher TOFE than radial networks.

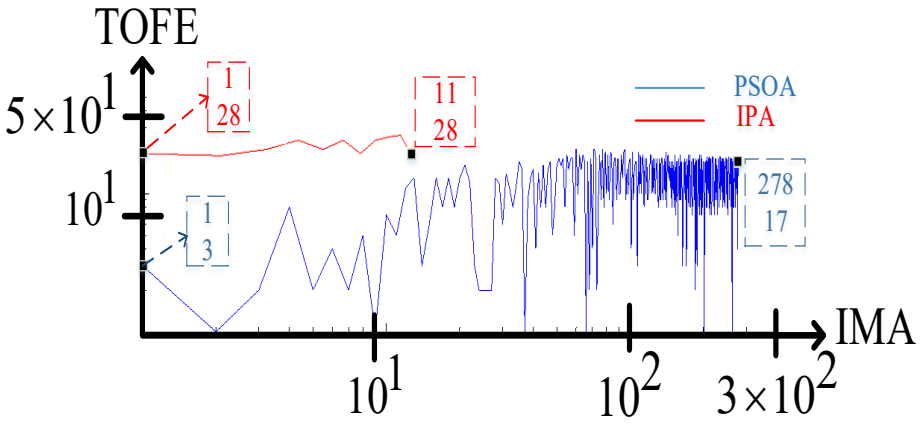


Figure 11. TOFE of the IPA and PSOA in the TESKO2 system.

4.5. Simulation Results: IEEE 14 Bus System

In this section, the IEEE 14 bus system will be considered to compare its results with four studies, including Refs. [1,5,6,12]. The technical details of the equipment for the IEEE 14 bus system are provided in Appendix C.

Here, only the findings of IPA for the IEEE 14 bus system are provided. The IEEE 14 bus network is comparable to the IEEE Std. 399-1997 and is more looped as a microgrid (the SAOA and PSOA are not converged in the IEEE Std. 399-1997 system). On the other hand, only IPA's outcomes are flawless, ending in a convergence of the problem for the IEEE 14 bus system.

All 20 components of the IEEE 14 bus system (illustrated in Figure 12) are susceptible to failure. They consist of five synchronous machines (two DGs and three generators), thirteen

lines (L1, . . ., L13), and two transformers (T1 and T2). However, only the equipment failures of the microgrid portion of the IEEE 14 bus system (shown in Figure 12) are considered in the studies referenced. According to (9), the IEEE 14 bus system's *N-2* contingencies result in 190 events. Despite this, as shown in Table A27 (provided in Appendix C), only eleven events are investigated as selected contingencies based on *N-K*-ESRT findings. It should be noted that the repeated contingencies for each bus can reduce the results of the *N-K*-ESRT obtained by (8). It should be noted that if the *N-K*-ESRT is not deployed on the POSP, it will not be possible to verify all of these topologies (i.e., 190 events), as calculating the setting parameters of DOCRs for each one is a time-consuming and laborious task.

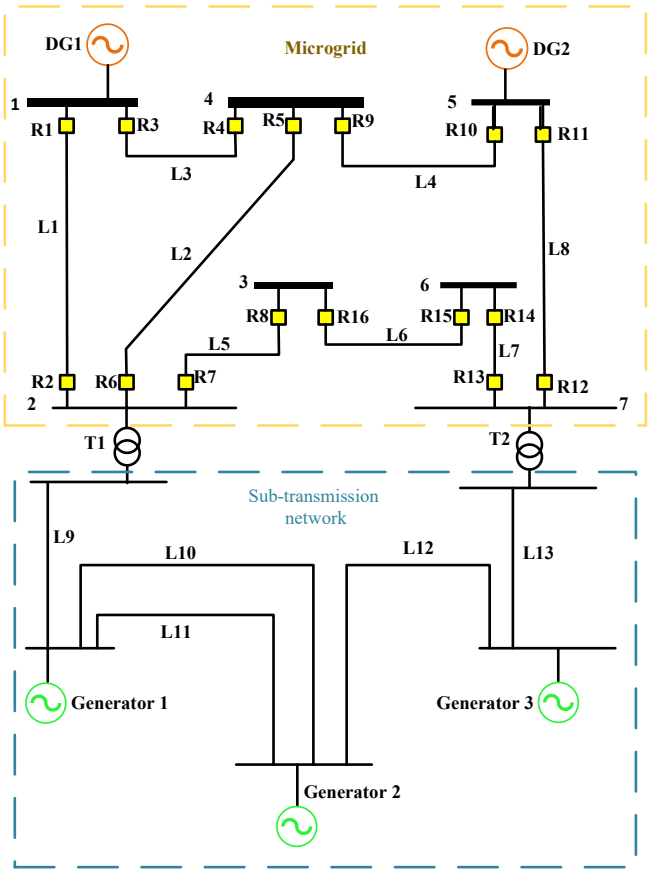


Figure 12. The IEEE 14 bus system.

Table 6 displays the tripping time (TT), ATT, and O-TSMP of all mounted DOCRs in the IEEE 14 bus system. These results are provided for various network topologies (four states), the methodology presented in this paper, and the referenced studies. Both ATT (or TT) and O-TSMP are provided for the proposed method of this paper; however, some columns in Table 6 are kept unfilled because only the results of these studies are presented. Four states are shown to be implemented on the IEEE 14 bus system in this table, including "FT" (state 1), "FT and *N-1* contingency" (state 2), "FT, *N-1* contingency, and island mode" (state 3), and "*N-2* contingencies" (state 4). Additionally, the findings of the method described in this paper are specified both with and without *N-K*-ESRT for easy comparison and taking decisions regarding the approach to the problem. As indicated previously, the large number of topological states resulting from *N-2* contingencies makes it impossible to implement this type of event without *N-K*-ESRT.

Table 6. Time results of previous studies compared to the proposed method of this paper in the IEEE 14 bus system.

STATE	The Proposed Method of This Paper without *N-K*-ESRT	The Proposed Method of This Paper with *N-K*-ESRT	[1]	[5]	[6]	[12]
1	TT = 7.765, O-TMSP = 2.013	TT = 7.765, O-TMSP = 2.013	TT = 8.366	TT = 14.062	-	TT = 11.058
2	ATT = 15.125, O-TMSP = 4.321	ATT = 12.598, O-TMSP = 3.487	-	ATT = 19.969	O-TMSP = 10.48	-
3	ATT = 20.213, O-TMSP = 6.558	ATT = 18.517, O-TMSP = 5.771	ATT = 49.783	-	-	-
4	-	ATT = 21.098, O-TMSP = 6.884	-	-	-	-

- stands for no data.

All four state outcomes demonstrate that the method proposed in this paper (even without *N-K*-ESRT) is markedly superior to those described in the aforementioned papers. The TT values of state 1, obtained by "the proposed method of this paper", [1], [5], and [12], are 7.765 s, 8.366 s, 14.062 s, and 11.058 s, respectively. First, it should be noted that in this state (state 1 = fixed topology), ATT, *N-K*-ESRT, and F-ZVCA are meaningless (since there is only one topology), and the results of this paper are identical with or without *N-K*-ESRT.

The sole consequence of this state is the convergence of the optimization algorithm. State one's findings indicate that the algorithm presented in this paper (IPA) and the parameters applied to it, as well as the objective function of the problem, worked well relative to other studies. For state 2, the procedure presented in this paper delivers the greatest results compared to the literature reviewed. The method proposed in this paper obtains an ATT of 15.125 s without *N-K*-ESRT and 12.598 s with *N-K*-ESRT, demonstrating the capability of *N-K*-ESRT. In addition, the O-TSMP value of the method presented in this paper without *N-K*-ESRT (4.321 s) is significantly lower than the value mentioned in [6] (10.48 s). The ATT determined by [1] for state 3 is 49.783 s, which corresponds to an operating time of 3.111 s per DOCR (because of the placement of sixteen DOCRs in the IEEE 14 bus system). However, the offered method of this paper with *N-K*-ESRT (18.517 s) and without *N-K*-ESRT (20.213 s) acquires the best results in state 3. Each relay's operating time (without *N-K*-ESRT) is 1.157 s, which is 1.95 s faster than [1]. It deserves to be noted that the island mode is one of the *N-2* outage modes (T1 and T2 outages) that leads to an exponential increase in the ATT. In the end, the approach outlined in this paper attains an ATT of 21.098 s for the *N-2* contingencies, which is employed by *N-K*-ESRT.

Finally, it can be concluded that IPA is the only algorithm that has produced stability in the meshed systems (including IEEE 14 bus and IEEE Std. 399-1997 networks). It was straightforward to determine whether the IPA was superior to other algorithms in terms of decreasing the time required for relays to trip and accelerating the rate of convergence of the POSP. In addition, an additional advantageous feature of the IPA is its extremely rapid MET. On the other hand, PSOA is recommended for the TESKO2 network due to its superior performance in comparison to the other MOAs.

5. Conclusions

The POSP of the DOCRs in light of the unpredictability of the power systems is one of the most important issues of the past decade. In addition, a number of references have investigated the optimal protective strategies for microgrids, taking into account various configurations, and a small number of studies have concentrated on all *N-1* contingency topologies. However, in none of the available references for the protection setting problem of DOCRs, there were no signs of solving techniques for the implementation of the *N-2* contingencies in POSP. This paper suggests *N-K*-ESRT in an effort to lower the scale of *N-2* events. Then, F-ZVCA serves to categorize these occurrences. Ultimately, PA-*CSP*-PB

and MOAs (SAOA, PSOA, and IPA) are utilized to acquire the DOCRs' *DSPs*. IPA is the only algorithm in the IEEE Std. 399-1997 and IEEE 14 bus networks that has contributed to convergence. The functionality of the IPA in this looped network in terms of DOCR's operating speed and the convergence of the *OF* were effectively assessed. In addition to the convergence of the *OF*, another major advantage of the IPA is its extreme MET, as all case studies demonstrate. For the TESKO2 grid, the PSOA is considered to be the most effective MOA in terms of relay operation time. In particular, the tendency for the IPA in the looped systems to converge demonstrates that the F-ZVCA works well. It should be highlighted that the failure of convergence in one of the clusters will lead to a shortage of coherence in POSP. Thus, in the event of inadequate coordination, a malfunction ensues, and the network does not maintain its stable level, contributing to interruptions in load or cascading failures. Yet, this issue can be resolved by incorporating concurrent contingencies into the POSP of DOCRs.

Author Contributions: H.K.Z. Conceptualization, methodology, software, validation, formal analysis, writing—original draft preparation, visualization. K.M.: validation, investigation, formal analysis, review and editing, supervision. A.B.: validation, formal analysis, review and editing, supervision. H.H.-D.: validation, formal analysis, review and editing, supervision. All authors have read and agreed to the published version of the manuscript.

Funding: This research received no external funding.

Institutional Review Board Statement: Not applicable.

Informed Consent Statement: Not applicable.

Data Availability Statement: All the data have been described in the text.

Conflicts of Interest: The authors declare no conflict of interest.

Nomenclature

μ	Set of main/backup DOCRs pairs	OT^S	Overall tripping time of main DOCRs (s)
M	Mth main DOCR; $M \in \{1, 2,\ldots,Q\}$	λ^S	Average ratio of the fault current of main DOCR to their backup relays (A)
JB	Jth backup DOCR (each main DOCR can have j backup relays)	DOT^{S-C}	Difference between OT^S and OT^C
S	The network structure (topology)	$\delta T^{MJB,S}$	Difference between the tripping times of main and its backup DOCRs (s)
N	Number of equipment assumed for outage	OCC	Number of permutations resulting from N-2 events
K	Number of previously failed equipment	$I_{FC}^{\mu,S}$	Fault current of main/backup DOCRs (A)
NB	Number of network buses	$I_{FC}^{M,S}$	Fault current of main DOCR (A)
$TSMP^{\mu,S}$	Time setting multiplier parameter of DOCR (Seconds (s))	$I_{FC}^{JB,S}$	Fault current of backup DOCRs (A)
$CSP^{\mu,S}$	Current setting parameter of DOCR (Ampere (A))	$I_{FCmin}^{\mu,S}$	Minimum fault current of main/backup DOCRs (A)
$T^{\mu,S}$	Tripping time of DOCR (s)	CTR^M	Current transformer ratio of main DOCR
$T^{JB,S}$	Tripping time of backup DOCR/DOCRs (s)	CTP^M	Number of primary winding turns of current transformer (CT) for main DOCR
$T^{M,S}$	Tripping time of main DOCR (s)	CTS^M	Number of secondary winding turns of CT for main DOCR
NU^{ESRT}	Number of 'N-2 events' resulting from the ESRT	I_{Pickup}^{M}	Maximum network current of main DOCR assumed for the procedure of achieving the CSP practical bound (A)
$I_{Loadmax}^{\mu,S}$	Maximum network current of main DOCR (A)	OT^C	Time center points of F-ZVCA (s)
I_{CSP}^{M}	Current passing through the secondary winding of CT for main DOCR (A)	λ^C	Fault current center locations of F-ZVCA
PS^M	Percentage of CT winding turns for main DOCR	$\omega\lambda^{S-C}$	Fuzzy parameter of F-ZVCA
NAB	Number of all network buses	$D\omega^{S-C}$	Comparison index of F-ZVCA

Appendix A. (TESKO2 Network Data)

Table A1. Technical data of each DG unit connected to the TESKO2 feeder.

Feature/Value	Parameter	Feature/Value	Parameter
3.498 pu	Synchronous reactance, X_d	Gas-engine	Generator type
0.2935 pu	Transient reactance, X'_d	2.2 MVA	Rated capacity
0.274 pu	Sub − transient reactance, X''_d	20 kV	Rated voltage
0.0419 pu	Zero − sequence reactance, X_0	50 Hz	Frequency
0.1531 pu	Negative − sequence reactance, X_2	0.93 lag	Nominal Power factor
Round-rotor	Rotor type	Directly grounded	Earthling type
1200 rpm	Nominal speed	0.9 lag–0.9 lead	Power factor range
4-wire YN		Winding connection	

Table A2. Technical data of EX connected to the TESKO2 feeder.

Feature/Value	Parameter	Feature/Value	Parameter
50 Hz	Frequency	20 Kv	Voltage
0.0258 pu	Impedance ratio, $\frac{R_0}{X_0}$	PQ	Corresponding Bus type
1 pu	Impedance ratio, $\frac{X_0}{X_1}$	1 pu	Impedance ratio, $\frac{Z_2}{Z_1}$

Table A3. Technical data of lines (per km) for the TESKO2 feeder.

Feature/Value	Parameter	Feature/Value	Parameter
0.11 Ohm	Positive − sequence reactance, X_1	Cable	Cable/OHL
0.13 Ohm	Positive − sequence resistance, R_1	20 kV	Rated voltage
0.11 Ohm	Negative − sequence reactance, X_2	0.815 kA	Rated current
0.13 Ohm	Negative − sequence resistance, R_2	50 Hz	Frequency
Aluminum	Conductor material	0.268 Ohm	Zero − sequence resistance, R_0
80 °C	Max. Operational Temperature	0.25 Ohm	Zero − sequence reactance, X_0

Table A4. Length of lines (Km) for the TESKO2 feeder.

L5	L4	L3	L2	L1	Line
0.32	0.277	0.268	0.731	0.856	Length

Table A5. Technical data of load$_a$ for the TESKO2 feeder.

Feature/Value	Parameter
Balance	Balance/Unbalance
2.125 MW	Active power
1.733 Mvar	Reactive power

Table A6. Technical data of $load_b$ for the TESKO2 feeder.

Feature/Value	Parameter
Balance	Balance/Unbalance
1.113 MW	Active power
0.71 Mvar	Reactive power

Table A7. Technical data of $load_c$ for the TESKO2 feeder.

Feature/Value	Parameter
Balance	Balance/Unbalance
0.325 MW	Active power
0.21 Mvar	Reactive power

Appendix B. (IEEE Std. 399-1997 Network Data)

Table A8. Technical data of DG1 unit connected to the IEEE Std. 399-1997 system.

Feature/Value	Parameter	Feature/Value	Parameter
2 pu	Synchronous reactance, X_d	Gas-engine	Generator type
0.3 pu	Transient reactance, X'_d	15.6 MVA	Rated capacity
0.128 pu	Sub − transient reactance, X''_d	13.8 kV	Rated voltage
0.057 pu	Zero − sequence reactance, X_0	60 Hz	Frequency
0.112 pu	Negative − sequence reactance, X_2	0.8 lag	Power factor
Round-rotor	Rotor type	Directly grounded	Earthling type
1200 rpm	Nominal speed	0.8 lag–0.8 lead	Power factor range
4-wire YN		Winding connection	

Table A9. Technical data of DG2 unit connected to the IEEE Std. 399-1997 system.

Feature/Value	Parameter	Feature/Value	Parameter
2 pu	Synchronous reactance, X_d	Gas-engine	Generator type
0.3 pu	Transient reactance, X'_d	12.5 MVA	Rated capacity
0.128 pu	Sub − transient reactance, X''_d	13.8 kV	Rated voltage
0.058 pu	Zero − sequence reactance, X_0	60 Hz	Frequency
0.128 pu	Negative − sequence reactance, X_2	0.8 lag	Nominal Power factor
Round-rotor	Rotor type	Directly grounded	Earthling type
1200 rpm	Nominal speed	0.8 lag–0.8 lead	Power factor range
4-wire YN		Winding connection	

Table A10. Technical data of EX connected to the IEEE Std. 399-1997 system.

Feature/Value	Parameter	Feature/Value	Parameter
60 Hz	Frequency	69 Kv	Voltage
0.0454 pu	Impedance ratio, $\frac{R_0}{X_0}$	PV	Corresponding Bus type
1 pu	Impedance ratio, $\frac{X_0}{X_1}$	1 pu	Impedance ratio, $\frac{Z_2}{Z_1}$

Table A11. Technical data of lines (i.e., L1, L2, L6. . . L20) (per km) for the IEEE Std. 399-1997 system.

Feature/Value	Parameter	Feature/Value	Parameter
0.12 Ohm	Positive − sequence reactance, X_1	Cable	Cable/OHL
0.144 Ohm	Positive − sequence resistance, R_1	13.8 kV	Rated voltage
0.12 Ohm	Negative − sequence reactance, X_2	0.315 kA	Rated current
0.144 Ohm	Negative − sequence resistance, R_2	60 Hz	Frequency
Aluminum	Conductor material	0.265 Ohm	Zero − sequence resistance, R_0
80 °C	Max. Operational Temperature	0.24 Ohm	Zero − sequence reactance, X_0

Table A12. Technical data of lines (i.e., L3, L4, L5) (per km) for the IEEE Std. 399-1997 system.

Feature/Value	Parameter	Feature/Value	Parameter
0.462 Ohm	Positive − sequence reactance, X_1	Overhead line (OHL)	Cable/OHL
0.217 Ohm	Positive − sequence resistance, R_1	69 kV	Rated voltage
0.462 Ohm	Negative − sequence reactance, X_2	0.251 kA	Rated current
0.217 Ohm	Negative − sequence resistance, R_2	60 Hz	Frequency
Aluminum	Conductor material	0	Zero − sequence resistance, R_0
80 °C	Max. Operational Temperature	0	Zero − sequence reactance, X_0

Table A13. Length of lines (Km) for the IEEE Std. 399-1997 system.

L20	L19	L18	L17	L16	L15	L14	L13	L12	L11	L10	L9	L8	L7	L6	L5	L4	L3	L2	L1	Line
0.55	0.19	0.19	0.15	0.15	0.36	0.18	0.29	0.14	0.2	0.09	0.14	0.06	0.003	0.05	3.048	0.6	3.048	0.6	0.6	Length

Appendix C. (IEEE 14 Bus Network Data)

Table A14. Technical data of each DG unit connected to the IEEE 14 bus system.

Feature/Value	Parameter	Feature/Value	Parameter
3.498 pu	Synchronous reactance, X_d	Gas-engine	Generator type
0.2935 pu	Transient reactance, X'_d	2.2 MVA	Rated capacity
0.274 pu	Sub − transient reactance, X''_d	33 kV	Rated voltage
0.0419 pu	Zero − sequence reactance, X_0	50 Hz	Frequency
0.1531 pu	Negative − sequence reactance, X_2	0.93 lag	Nominal Power factor
Round-rotor	Rotor type	Directly grounded	Earthling type
1200 rpm	Nominal speed	0.9 lag–0.9 lead	Power factor range
4-wire YN		Winding connection	

Table A15. Technical data of generator 1 connected to the IEEE 14 bus system.

Feature/Value	Parameter	Feature/Value	Parameter
50 Hz	Frequency	132 Kv	Voltage
2 pu	Synchronous reactance, X_d	SL	Corresponding Bus type
0.3 pu	Transient reactance, X'_d	YN	Winding connection
0.2 pu	Sub − transient reactance, X''_d	0.8	Power factor
0.2 pu	Negative − sequence reactance, X_2	0.1 pu	Zero − sequence reactance, X_0

Table A16. Technical data of generator 2 connected to the IEEE 14 bus system.

Feature/Value	Parameter	Feature/Value	Parameter
50 Hz	Frequency	132 Kv	Voltage
2 pu	Synchronous reactance, X_d	PV	Corresponding Bus type
0.3 pu	Transient reactance, X'_d	YN	Winding connection
0.2 pu	Sub − transient reactance, X''_d	0.8	Power factor
0.2 pu	Negative − sequence reactance, X_2	0.1 pu	Zero − sequence reactance, X_0

Table A17. Technical data of generator 3 connected to the IEEE 14 bus system.

Feature/Value	Parameter	Feature/Value	Parameter
50 Hz	Frequency	132 Kv	Voltage
2 pu	Synchronous reactance, X_d	PV	Corresponding Bus type
0.3 pu	Transient reactance, X'_d	23.4 Mvar	Reactive power
0.2 pu	Sub − transient reactance, X''_d	0.8	Power factor
0.2 pu	Negative − sequence reactance, X_2	0.1 pu	Zero − sequence reactance, X_0
YN		Winding connection	

Table A18. Technical data of line 1 (i.e., L1) for the IEEE 14 bus system.

Feature/Value	Parameter	Feature/Value	Parameter
2.785 Ohm	Positive − sequence reactance, X_1	OHL	Cable/OHL
1.338 Ohm	Positive − sequence resistance, R_1	33 kV	Rated voltage
2.785 Ohm	Negative − sequence reactance, X_2	1 kA	Rated current
1.338 Ohm	Negative − sequence resistance, R_2	50 Hz	Frequency
Copper	Conductor material	0 Ohm	Zero − sequence resistance, R_0
80 °C	Max. Operational Temperature	0 Ohm	Zero − sequence reactance, X_0

Table A19. Technical data of line 2 (i.e., L2) for the IEEE 14 bus system.

Feature/Value	Parameter	Feature/Value	Parameter
1.418 Ohm	Positive − sequence reactance, X_1	OHL	Cable/OHL
0.72 Ohm	Positive − sequence resistance, R_1	33 kV	Rated voltage
1.418 Ohm	Negative − sequence reactance, X_2	1 kA	Rated current
0.72 Ohm	Negative − sequence resistance, R_2	50 Hz	Frequency
Copper	Conductor material	0 Ohm	Zero − sequence resistance, R_0
80 °C	Max. Operational Temperature	0 Ohm	Zero − sequence reactance, X_0

Table A20. Technical data of line 3 (i.e., L3) for the IEEE 14 bus system.

Feature/Value	Parameter	Feature/Value	Parameter
2.176 Ohm	Positive − sequence reactance, X_1	OHL	Cable/OHL
2.405 Ohm	Positive − sequence resistance, R_1	33 kV	Rated voltage
2.176 Ohm	Negative − sequence reactance, X_2	1 kA	Rated current
2.405 Ohm	Negative − sequence resistance, R_2	50 Hz	Frequency
Copper	Conductor material	0 Ohm	Zero − sequence resistance, R_0
80 °C	Max. Operational Temperature	0 Ohm	Zero − sequence reactance, X_0

Table A21. Technical data of line 4 (i.e., L4) for the IEEE 14 bus system.

Feature/Value	Parameter	Feature/Value	Parameter
3.789 Ohm	Positive − sequence reactance, X_1	OHL	Cable/OHL
1.861 Ohm	Positive − sequence resistance, R_1	33 kV	Rated voltage
3.789 Ohm	Negative − sequence reactance, X_2	1 kA	Rated current
1.861 Ohm	Negative − sequence resistance, R_2	50 Hz	Frequency
Copper	Conductor material	0 Ohm	Zero − sequence resistance, R_0
80 °C	Max. Operational Temperature	0 Ohm	Zero − sequence reactance, X_0

Table A22. Technical data of line 5 (i.e., L5) for the IEEE 14 bus system.

Feature/Value	Parameter	Feature/Value	Parameter
2.166 Ohm	Positive − sequence reactance, X_1	OHL	Cable/OHL
1.034 Ohm	Positive − sequence resistance, R_1	33 kV	Rated voltage
2.166 Ohm	Negative − sequence reactance, X_2	1 kA	Rated current
1.034 Ohm	Negative − sequence resistance, R_2	50 Hz	Frequency
Copper	Conductor material	0 Ohm	Zero − sequence resistance, R_0
80 °C	Max. Operational Temperature	0 Ohm	Zero − sequence reactance, X_0

Table A23. Technical data of line 6 (i.e., L6) for the IEEE 14 bus system.

Feature/Value	Parameter	Feature/Value	Parameter
2.091 Ohm	Positive − sequence reactance, X_1	OHL	Cable/OHL
0.893 Ohm	Positive − sequence resistance, R_1	33 kV	Rated voltage
2.091 Ohm	Negative − sequence reactance, X_2	1 kA	Rated current
0.893 Ohm	Negative − sequence resistance, R_2	50 Hz	Frequency
Copper	Conductor material	0 Ohm	Zero − sequence resistance, R_0
80 °C	Max. Operational Temperature	0 Ohm	Zero − sequence reactance, X_0

Table A24. Technical data of line 7 (i.e., L7) for the IEEE 14 bus system.

Feature/Value	Parameter	Feature/Value	Parameter
0.92 Ohm	Positive − sequence reactance, X_1	OHL	Cable/OHL
0.346 Ohm	Positive − sequence resistance, R_1	33 kV	Rated voltage
0.92 Ohm	Negative − sequence reactance, X_2	1 kA	Rated current
0.346 Ohm	Negative − sequence resistance, R_2	50 Hz	Frequency
Copper	Conductor material	0 Ohm	Zero − sequence resistance, R_0
80 °C	Max. Operational Temperature	0 Ohm	Zero − sequence reactance, X_0

Table A25. Technical data of transformer 1 (T1) for the IEEE 14 bus system.

Feature/Value	Parameter	Feature/Value	Parameter
0.252 Ohm	Positive − sequence reactance, X_1	YN/yn0	Connection
0.5 pu	Leakage reactance	132 kV/33 kV	Rated voltage
0.5 pu	Leakage resistance	50 Hz	Frequency

Table A26. Technical data of transformer 2 (T2) for the IEEE 14 bus system.

Feature/Value	Parameter	Feature/Value	Parameter
0.556 Ohm	Positive − sequence reactance, X_1	YN/yn0	Connection
0.5 pu	Leakage reactance	132 kV/33 kV	Rated voltage
0.5 pu	Leakage resistance	50 Hz	Frequency
YN/yn0	Connection	50 Hz	Frequency

Table A27. The results of *N-K*-ESRT for the IEEE 14 bus system.

Bus		EV	VFT	EN
Bus 1	UB	1.314	1.104	L1-L3
	LB	1.058		L2-DG1
Bus 2	UB	1.177	1.070	Generator1-T1
	LB	1.070		FT
Bus 3	UB	1.187	1.087	Generator1-L8
	LB	1.087		FT
Bus 4	UB	1.269	1.092	L1-L3
	LB	1.058		DG1-DG2
Bus 5	UB	1.301	1.113	L3-L6
	LB	1.051		T1-T2
Bus 6	UB	1.151	1.075	Generator1-T2
	LB	1		T1-T2
Bus 7	UB	1.150	1.078	Generator1-T2
	LB	1.078		FT

References

1. Saleh, K.A.; Mehrizi-Sani, A. Harmonic directional overcurrent relay for islanded microgrids with inverter-based DGs. *IEEE Syst. J.* **2020**, *15*, 2720–2731. [CrossRef]
2. El-Sayed, W.T.; Azzouz, M.A.; Zeineldin, H.H.; El-Saadany, E.F. A harmonic time-current-voltage directional relay for optimal protection coordination of inverter-based islanded microgrids. *IEEE Trans. Smart Grid* **2020**, *12*, 1904–1917. [CrossRef]
3. Sati, T.E.; Azzouz, M.A. Optimal protection coordination for inverter dominated islanded microgrids considering N-1 contingency. *IEEE Trans. Power Deliv.* **2021**, *37*, 2256–2267. [CrossRef]
4. Wu, D.; Kalathil, D.; Begovic, M.M.; Ding, K.Q.; Xie, L. Deep reinforcement learning-based robust protection in DER-rich distribution grids. *IEEE Open Access J. Power Energy* **2022**, *9*, 537–548. [CrossRef]
5. Alam, M.N.; Chakrabarti, S.; Pradhan, A.K. Protection of networked microgrids using relays with multiple setting groups. *IEEE Trans. Ind. Inform.* **2022**, *18*, 3713–3723. [CrossRef]
6. Ojaghi, M.; Mohammadi, V. Use of clustering to reduce the number of different setting groups for adaptive coordination of overcurrent relays. *IEEE Trans. Power Deliv.* **2018**, *33*, 1204–1212. [CrossRef]
7. Ghotbi-Maleki, M.; Chabanloo, R.M.; Zeineldin, H.H.; Hosseini Miangafsheh, S.M. Design of setting group-based overcurrent protection scheme for active distribution networks using MILP. *IEEE Trans. Smart Grid* **2021**, *12*, 1185–1193. [CrossRef]

8. Shafaghatian, N.; Heidary, A.; Radmanesh, H.; Rouzbehi, K. Microgrids interconnection to upstream AC grid using a dual-function fault current limiter and power flow controller: Principle and test results. *IET Energy Syst. Integr.* **2019**, *1*, 269–275. [CrossRef]
9. Khurshaid, T.; Wadood, A.; Gholami Farkoush, S.; Kim, C.H.; Yu, J.; Rhee, S.B. Improved firefly algorithm for the optimal coordination of directional overcurrent relays. *IEEE Access* **2019**, *7*, 78503–78514. [CrossRef]
10. Korashy, A.; Kamel, S.; Alquthami, T.; Jurado, F. Optimal coordination of standard and non-standard direction overcurrent relays using an improved moth-flame optimization. *IEEE Access* **2020**, *8*, 87378–87392. [CrossRef]
11. Alaee, P.; Amraee, T. Optimal coordination of directional overcurrent relays in meshed active distribution network using imperialistic competition algorithm. *J. Mod. Power Syst. Clean Energy* **2021**, *9*, 416–422. [CrossRef]
12. Abdelhamid, M.; Houssein, E.H.; Mahdy, M.A.; Selim, A.; Kamel, S. An improved seagull optimization algorithm for optimal coordination of distance and directional over-current relays. *Expert Syst. Appl.* **2022**, *200*, 116931. [CrossRef]
13. Acharya, D.; Das, D.K. An efficient optimizer for optimal overcurrent relay coordination in power distribution system. *Expert Syst. Appl.* **2022**, *199*, 116858. [CrossRef]
14. Idarraga-Ospina, G.; Mesa-Quintero, N.A.; Valencia, J.A.; Cavazos, A.; Orduna, E. Directional overcurrent relay coordination by means of genetic algorithms of Chu-Beasley. *IEEJ Trans. Electr. Electron. Eng.* **2018**, *13*, 522–528. [CrossRef]
15. Tightiz, L.; Mansouri, S.; Zishan, F.; Yoo, J.; Shafaghatian, N. Maximum power point tracking for photovoltaic systems operating under partially shaded conditions using SALP swarm algorithm. *Energies* **2022**, *15*, 8210. [CrossRef]
16. Ataee-Kachoee, A.; Hashemi-Dezaki, H.; Ketabi, A. Optimized adaptive protection coordination of microgrids by dual-setting directional overcurrent relays considering different topologies based on limited independent relays' setting groups. *Electr. Power Syst. Res.* **2023**, *214*, 108879. [CrossRef]
17. Tiwari, R.; Singh, R.K.; Choudhary, N.K. Coordination of dual setting overcurrent relays in microgrid with optimally determined relay characteristics for dual operating modes. *Prot. Control Mod. Power Syst.* **2022**, *7*, 6. [CrossRef]
18. Alasali, F.; Saidi, A.S.; El-Naily, N.; Smadi, M.A.; Holderbaum, W. Hybrid tripping characteristic-based protection coordination scheme for photovoltaic power systems. *Sustainability* **2023**, *15*, 1540. [CrossRef]
19. Khurshaid, T.; Wadood, A.; Gholami Farkoush, S.; Yu, J.; Kim, C.H.; Rhee, S.B. An improved optimal solution for the directional overcurrent relays coordination using hybridized whale optimization algorithm in complex power systems. *IEEE Access* **2019**, *7*, 90418–90435. [CrossRef]
20. Agwa, A.M.; El-Fergany, A.A. Protective Relaying Coordination in Power Systems Comprising Renewable Sources: Challenges and Future Insights. *Sustainability* **2023**, *15*, 7279. [CrossRef]
21. Zand, H.K.; Mazlumi, K.; Bagheri, A. Protection coordination for micro-grids based on multi-objective optimization considering simultaneous uncertainty. In Proceedings of the 2019 International Conference on Protection and Automation of Power System (IPAPS), Tehran, Iran, 8–9 January 2019; IEEE: New York, NY, USA, 2019; pp. 7–11. [CrossRef]
22. Kida, A.A.; Labrador Rivas, A.E.; Gallego, L.A. An improved simulated annealing–linear programming hybrid algorithm applied to the optimal coordination of directional overcurrent relays. *Electr. Power Syst. Res.* **2020**, *181*, 106197. [CrossRef]
23. Labrador Rivas, A.E.; Gallego Pareja, L.A.; Abrão, T. Coordination of distance and directional overcurrent relays using an extended continuous domain ACO algorithm and an hybrid ACO algorithm. *Electr. Power Syst. Res.* **2019**, *170*, 259–272. [CrossRef]
24. Rizk-Allah, R.M.; El-Fergany, A.A. Effective coordination settings for directional overcurrent relay using hybrid Gradient-based optimizer. *Appl. Soft Comput.* **2021**, *112*, 107748. [CrossRef]
25. Draz, A.; Elkholy, M.M.; El-Fergany, A. Over-current relays coordination including practical constraints and DGs: Damage curves, inrush, and starting currents. *Sustainability* **2022**, *14*, 2761. [CrossRef]
26. Choudhary, P.K.; Das, D.K. Optimal coordination of over-current relay in a power distribution network using opposition based learning fractional order class topper optimization (OBL-FOCTO) algorithm. *Appl. Soft Comput.* **2021**, *113*, 107916. [CrossRef]
27. Alam, M.N. Adaptive Protection Coordination Scheme Using Numerical Directional Overcurrent Relays. *IEEE Trans. Ind. Inform.* **2019**, *15*, 64–73. [CrossRef]
28. Mahindara, V.R.; Rodriguez, D.F.C.; Pujiantara, M.; Priyadi, A.; Purnomo, M.H.; Muljadi, E. Practical challenges of inverse and definite-time overcurrent protection coordination in modern industrial and commercial power distribution system. *IEEE Trans. Ind. Appl.* **2021**, *57*, 187–197. [CrossRef]
29. Ramli, S.P.; Pashaei, M.; Karimi, M.; Kauhaniemi, K.; Pourdaryaei, A.; Daryaei, M.; Zarei, M. The recent development of optimal DOCR protection strategies for sustainable power systems via computational intelligence techniques. *IEEE Access* **2022**, *10*, 134277–134291. [CrossRef]
30. Darabi, A.; Bagheri, M.B.; Gharehpetian, G. Highly sensitive microgrid protection using overcurrent relays with a novel relay characteristic. *IET Renew. Power Gener.* **2020**, *14*, 1201–1209. [CrossRef]
31. Ramli, S.P.; Mokhlis, H.; Wong, W.R.; Muhammad, M.A.; Mansor, N.N. Optimal coordination of directional overcurrent relay based on combination of Firefly Algorithm and Linear Programming. *Ain Shams Eng. J.* **2022**, *13*, 101777. [CrossRef]
32. Karimkhan Zand, H.; Mazlumi, K.; Bagheri, A. A new approach for the setting of directional overcurrent relays by incorporating cascading outages. *Sci. Iran.* **2022**, *29*, 1562–1572. [CrossRef]

33. Usama, M.; Mokhlis, H.; Mansor, N.N.; Moghavvemi, M.; Akhtar, M.N.; Bajwa, A.A.; Awalin, L.J. A multi-objective optimization of FCL and DOCR settings to mitigate distributed generations impacts on distribution networks. *Int. J. Electr. Power Energy Syst.* **2023**, *147*, 108827. [CrossRef]
34. Noghabi, A.S.; Mashhadi, H.R.; Sadeh, J. Optimal coordination of directional overcurrent relays considering different network topologies using interval linear programming. *IEEE Trans. Power Deliv.* **2010**, *25*, 1348–1354. [CrossRef]
35. Li, C.; Sun, Y.; Chen, X. Recommendations to improve power system security: Lessons learned from the Europe blackout on November 4. In Proceedings of the 2007 42nd International Universities Power Engineering Conference, Brighton, UK, 4–6 September 2007; pp. 529–533. [CrossRef]
36. Xue, Y.; Xiao, S. Generalized congestion of power systems: Insights from the massive blackouts in India. *J. Mod. Power Syst. Clean Energy* **2013**, *1*, 91–100. [CrossRef]
37. Regional Group Nordic. *Nordic and Baltic Grid Disturbance Statistics 2020*; ENTSO-E: Brussels, Belgium, 2021.
38. Multifunction Protection with Synchronization-SIPROTEC 7SJ64. Siemens.com Global Website. Available online: https://www.siemens.com/global/en/products/energy/energy-automation-and-smart-grid/protection-relays-and-control/siprotec-4/overcurrent-and-motor-protection/multifunction-protection-with-synchronization-siprotec-7sj64.html (accessed on 21 July 2023).
39. Zhang, X.; Wang, Z.; Lu, Z. Multi-objective load dispatch for microgrid with electric vehicles using modified gravitational search and particle swarm optimization algorithm. *Appl. Energy* **2022**, *306*, 118018. [CrossRef]
40. Deng, W.; Zhang, Y.; Tang, Y.; Li, Q.; Yi, Y. A neural network-based adaptive power-sharing strategy for hybrid frame inverters in a microgrid. *Front. Energy Res.* **2023**, *10*, 1082948. [CrossRef]
41. Shao, B.; Xiao, Q.; Xiong, L.; Wang, L.; Yang, Y.; Chen, Z.; Guerrero, J.M. Power coupling analysis and improved decoupling control for the VSC connected to a weak AC grid. *Int. J. Electr. Power Energy Syst.* **2023**, *145*, 108645. [CrossRef]
42. Zand, H.K.; Mazlumi, K.; Bagheri, A.; Abdali, A. Optimal coordination of DOCRs in microgrid via contingency reduction mech-anism and clustering algorithms considering various network topologies based on N-2 contingencies. *Expert Syst. Appl.* **2023**, *234*, 121061. [CrossRef]
43. Li, J.; Deng, Y.; Sun, W.; Li, W.; Li, R.; Li, Q.; Liu, Z. Resource orchestration of cloud-edge–based smart grid fault detection. *ACM Trans. Sens. Netw.* **2022**, *18*, 1–26. [CrossRef]
44. Taghieh, A.; Mohammadzadeh, A.; Zhang, C.; Kausar, N.; Castillo, O. A type-3 fuzzy control for current sharing and voltage balancing in microgrids. *Appl. Soft Comput.* **2022**, *129*, 109636. [CrossRef]
45. Cao, B.; Dong, W.; Lv, Z.; Gu, Y.; Singh, S.; Kumar, P. Hybrid microgrid many-objective sizing optimization with fuzzy decision. *IEEE Trans. Fuzzy Syst.* **2020**, *28*, 2702–2710. [CrossRef]
46. Myrvold, W.C. *Beyond Chance and Credence: A Theory of Hybrid Probabilities*; Oxford University Press: Oxford, UK, 2021.
47. *IEC 60909-0*; Short-Circuit Currents in Three-Phase a.c. Systems—Part 0: Calculation of Currents. IEC: Geneva, Switzerland, 2016.
48. Global Optimization Toolbox; Mathworks.com. Available online: https://www.mathworks.com/help/gads/ (accessed on 28 April 2023).
49. Find Minimum of Function Using Pattern Search-MATLAB Pattern Search, Mathworks.com. Available online: https://www.mathworks.com/help/gads/patternsearch.html (accessed on 28 April 2023).
50. Tolerances and Stopping Criteria—MATLAB & Simulink; Mathworks.com. Available online: https://www.mathworks.com/help/optim/ug/tolerances-and-stopping-criteria.html (accessed on 28 April 2023).
51. Power Systems Test Case Archive; Ece.uw.edu. Available online: https://labs.ece.uw.edu/pstca/ (accessed on 25 May 2013).

Disclaimer/Publisher's Note: The statements, opinions and data contained in all publications are solely those of the individual author(s) and contributor(s) and not of MDPI and/or the editor(s). MDPI and/or the editor(s) disclaim responsibility for any injury to people or property resulting from any ideas, methods, instructions or products referred to in the content.